frontiers | Frontiers in Earth Science

TYPE Original Research
PUBLISHED 13 January 2023
DOI 10.3389/feart.2022.991304

OPEN ACCESS

EDITED BY
Junjian Zhang,
Shandong University of Science and Technology, China

REVIEWED BY
Fangkai Quan,
China University of Mining and Technology, China
Zhihui Ma,
Sichuan University of Science and Engineering, China

*CORRESPONDENCE
Minggao Yu,
13333910808@126.com

SPECIALTY SECTION
This article was submitted to Economic Geology, a section of the journal Frontiers in Earth Science

RECEIVED 11 July 2022
ACCEPTED 30 August 2022
PUBLISHED 13 January 2023

CITATION
Teng F, Yu M, Han X and Chao J (2023), Study on the mechanism of coal pillar breaking and fracture development under repeated mining in a close seam group.
Front. Earth Sci. 10:991304.
doi: 10.3389/feart.2022.991304

Study on the mechanism of coal pillar breaking and fracture development under repeated mining in a close seam group

Fei Teng[1], Minggao Yu[1,2]*, Xuefeng Han[1] and Jiangkun Chao[2]

[1]School of Safety Science and Engineering, Henan Polytechnic University, Jiaozuo, China, [2]State Key Laboratory of Coal Mine Disaster Dynamics and Control, Chongqing University, Chongqing, China

The study show the influence of coal mining on pillar under a repeated mining, in a close coal seam group, the fracture and instability process and influence mechanism of fracture development on the oxidation of coal pillars. In this paper, FLAC^{3D} numerical simulation software is used to simulate the dynamic evolution characteristics of stress, displacement of the upper coal pillar. The results show that 1) The theoretical length of the fracture along the strike of the upper coal pillar is obtained by establishing the mechanical model of the upper coal pillar, which is consistent with the numerical simulation results. 3) In this paper, according to the dynamic evolution characteristics of displacement and stress on the coal pillar, the coal pillar is divided into the "step subsidence area", "fracture compaction area" and "reverse stress area", and the high risk area of the coal spontaneous combustion is determined.

KEYWORDS

fire and explosion, coal, coal spontaneous combustibility, fracture, cracks, rock and coal system

1 Introduction

Coal spontaneous combustion is a serious problem of coal mining (Ramani, 1997; Wactawi, 1998; Wang et al., 2003; Genc and Cook, 2015). Some important coalfields in China, there are a huge number of shallow buried depth of 80–240 m coal, the mining of them will lead to a large area of land subsidence and destroy the local ecological environment. Some scholars (Ju and Xu, 2015; Bi et al., 2019; Chen et al., 2019) take a series of field monitoring and comparisons with previous studies. Some scholars introduces a new profile function method for prediction of surface subsidence due to inclined coal-seam mining and use DInSAR technology to identify and monitoring subsidence basins caused by underground coal mining activities (Asadi et al., 2005; Przylucka et al., 2015). Flac3D software were used to simulate the actual geological conditions and improve insufficiency of the classical method according to the simulate results, which confirm the Flac3D is a simple and effective way predict surface mining displacement (Xie and Zhou, 1999). The surface subsidence caused by coal mining threatens the local ecological environment seriously.

The occurrence characteristics of shallow buried and close distances of coal seams, which make the coal remaining in goaf vulnerable to the influence of the mining of adjacent coal seam, which form a leakage passage through the working face, gob and surface, some scholar measured the displacement, stress changes of strata in the process of longwall mining and monitored them, and simulated the stress and permeability changes of strata, and study the distribution and evolution of displacement, fracture and stress through similar material simulation test. (Ma et al., 2013; Guo et al., 2012; Kidybinski and Babcock, 1973; Majdi et al., 2012; Prucz et al., 1989; Li et al., 2013). The mining-induced cracks, which leads to air leakage caused by the repeated mining of shallow coal seams a, and a similar simulation experiment was carried out in the laboratory, and then the ground mining-induced cracks were observed and the crack air leakage was detected. As the source of air leakage in the goaf, these cracks through the surface greatly increase the possibility of coal spontaneous combustion disaster in the goaf (Lu and Qin, 2015; Cheng et al., 2017; Hao et al., 2019; Wang et al., 2019; Zhuo et al., 2019).

In the mining process, the stability of the pillar will be affected by mining disturbances in the next adjacent layer and will be in a state of dynamic balance or even fracture instability. (Huang and Cao, 2019; Pan et al., 2017; Liu et al., 2016; Liu, 2019; Wang et al., 2018a; Wang et al., 2018b). The key characterization parameters and functional relationship that affect the permeability change of coal bodies through experimental research and theoretical analysis, providing theoretical support for the oxidation and spontaneous combustion characteristics of coal bodies under different stress loading paths. Through the establishment of a unified mathematical model to describe the permeability of coal pores and fractures, the gas seepage in coal can be divided into three types: pore control type, fracture control type and pore fracture joint control type (Jaiswal and Shrivastva, 2009; Wattimena et al., 2013).

At present, research on spontaneous coal combustion is mainly focused on the prevention and control of remaining coal in a goaf; however, there is little mention of that the coal pillars spontaneous combustion. Obviously, coal pillar of the goaf is a core area of spontaneous combustion of shallow buried and close-distance coal seams. Therefore, studying the mechanism of the breaking and oxidation of the coal pillar in the upper goaf can guide the prevention and control of spontaneous coal combustion.

By using FLAC^{3D} numerical simulation software to simulate the dynamic excavation process and combining with the change law of the plastic area and displacement of the pillar, this paper explores the fracture development and breaking mechanism of the pillar in the repeated mining process and judges the high-risk area of spontaneous combustion of it of the upper coal seam. The prevention and control of spontaneous combustion in the goaf is of great practical significance.

2 Numerical model and parameter setting

2.1 Model establishment

The physics model was established in accordance with the working face drilling histogram of the Bulianta Coal Mine. There were three mining faces (A, B, C and D) with lengths of 300 m and a face C with a length of 400 m. Additionally, 100–200 m of coal remained on both sides of the boundary tunnel to avoid the boundary effect. The mining was conducted according to the order of the mining faces (A, B, C and D). There was a coal pillar (about 40 m) between A and B, and the coal pillar of the lower coal seam was staggered with the coal pillar of the upper coal seam by 100 m. The simulated conditions of the recovery are shown in Table 1, and the model is shown in Figure 1.

2.2 Mechanical parameter setting and simulation scheme

According to the distribution of rock strata in the working face (Li et al., 2016), the mechanical parameters of each rock mass are determined. Mohr Coulomb yield criterion is adopted for model calculation. See Table 2 for physical and mechanical parameters of coal and rock mass in each layer.

3 Results and discussion

3.1 Stress distribution at different mining stages

Figures 2, 3 show the *z*-direction stress distribution map of the top and bottom surfaces of the coal pillar after the mining of working faces A, B, C and D. In different mining stages, the comparative distribution of stress at the top and bottom of coal pillar along the strike of 140 and 250 m is shown in Figures 4, 5, 6, 7. FLAC^{3D} specifies that the direction of the force is negative downward and positive upward along the *z*-direction.

3.1.1 Completion of stope A

Stress concentration is formed along one side of the goaf of the coal body, and the maximum stress at the top of the coal pillar is 8–8.3 mpa. With the increase of the distance between the coal body and the goaf, the stress on the coal body decreases. At the left boundary, the stress slightly increased compared with the original rock stress. There is an obvious stress concentration area along the coal pillar 565–585 m dip angle, with a stress of 6–7 MPa at 590–595 m along the dip. The stress decreases to approximately 5.9 MPa; along

TABLE 1 Simulated condition of recovery.

Working face	depth/m	Strike length/m	Dip length/m	Coal thickness/m	Mining thickness/m
A	162	300	300	5.5	4.5
B	162	300	300	5.5	4.5
C	192	300	400	6.2	5
D	192	300	300	6.2	5

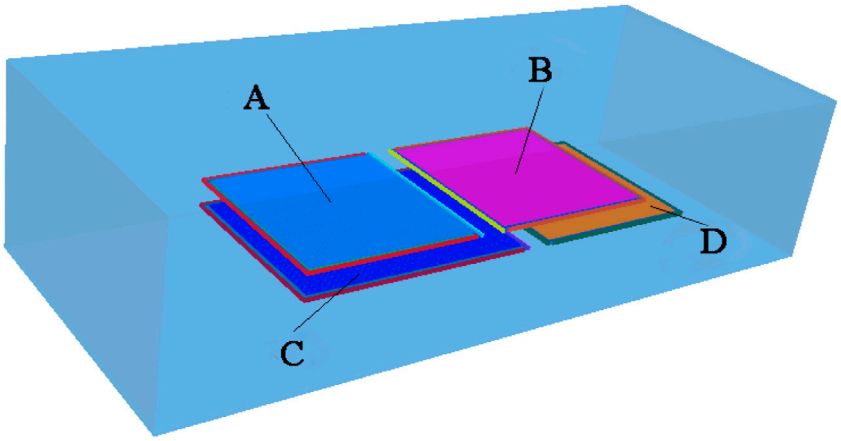

FIGURE 1
The coal mine excavation model.

the incline from 590 to 600 m, the stress concentration zone running through the strike appears again at the bottom of the coal pillar. When mining face A is completed, the variation trend of stress at the bottom of the coal pillar is quite different from that at the top of the coal pillar.

3.1.2 Completion of stope B

The *z*-direction stress on the top surface of the coal pillar is basically distributed symmetrically, and the maximum stress value along the goaf on both sides of the coal pillar is approximately 10 MPa. The minimum *z*-direction stress in the middle of the core area of the coal pillar is approximately 7.4 MPa. The stress distribution at the bottom of the coal pillar is basically the same as that at the top, but the stress concentration at the bottom appears at 100–150 and 350–400 m along the strike of the coal pillar, and the minimum *z*-direction stress in the middle of the core area of the coal pillar is approximately 7.4 MPa.

3.1.3 Completion of stope C

The coal pillar of the upper coal seam is in the disturbed fracture zone of the lower coal seam, and the mining of the lower coal seam leads to a new balance of the coal pillar of the upper coal seam. At this time, 200–300 m along the strike of the left side of the coal pillar is the place with the largest stress on the top of the whole coal pillar, and the maximum stress is approximately 4 MPa. Taking this as the centre, the absolute value of the stress decreases in an elliptical wave to the right until the stress value at the right boundary of the coal pillar reaches 1.5 MPa, and the stress direction is downward.

At 125–175 and 325–375 m along the strike of the right boundary of the coal pillar, the *z*-direction stress on the top surface of the coal pillar changes from vertical downward to vertical upward, and the stress value is approximately 0.2 MPa. The recovery of face C is a pressure relief process for the coal pillar of the upper coal seam. In this process, the stress on the top of the coal pillar drops below the stress of the primary rock, and the stress direction in some areas has changed. The stress distribution of the coal pillar bottom and top is consistent; taking the left side of the coal pillar as the centre along the strike of 200–300 m, the absolute value of stress decreases to the right, the value of stress at the right boundary of the coal pillar reaches 1–1.4 MPa, and the direction of stress is downward. At 125–175 and 325–375 m along the strike of the coal pillar, the

TABLE 2 The mechanical parameters of coal and rock.

Strata	Burying depth/m	Density/kg·m-3	Modulus of elasticity/GPa	Friction angle/°	Cohesion/MPa	Tensile strength/MPa	Poisson's ratio/°
Aeolian sand	17	1,450		24.7	1.0	1.0	0.26
Sandy mudstone	41	2,250	1.52	28.6	1.1	0.7	0.28
Siltstone	43	2050	2.31	30.8	6.5	1.77	0.27
Mudstone	62	2,600	1.9	33.1	2.2	1.01	0.25
Fine sandstone	71	2090	1.15	23.4	2.8	0.75	0.27
Medium grain sandstone	76	2050	0.43	29.8	8.31	2.62	0.26
Fine sandstone	81	2,219	1.27	22.3	1.26	0.49	0.27
Siltstone	87	2,313	0.81	34.1	1.16	1.75	0.31
Fine sandstone	124	2,295	16.04	26.8	9.31	4.28	0.16
Sandy mudstone	134	2,334	14.34	24.7	6.28	1.78	0.29
Mudstone	139	2,326	4.08	26	10.12	2.76	0.28
Coarse-grained sandstone	155	2,204	6.71	19.5	12.4	1.33	0.23
1–2 coal seam	16	1,284	1.76	23.6	17.9	1.68	0.27
Sandy mudstone	177	2,308	7.27	26.1	18.96	5.24	0.26
Fine sandstone	181	2,226	7.39	24.5	14.68	3.38	0.24
Coarse-grained sandstone	190	2,185	3.88	14.1	27.6	2.88	0.27
2–2 coal seam	195	1,303	1.99	24.5	19.25	1.17	0.23

z-direction stress direction of the coal pillar bottom changed from downward along the *z*-direction to upward along the *z*-direction, and the stress value was 0.2 MPa.

3.1.4 Completion of stope D

The maximum stress is 7.5 MPa on the left side of the top of coal pillar along the strike of 200–300 m; it decreases to the right and reaches approximately 5 MPa at the right boundary of coal pillar, and the stress on the top of the coal pillar increases to more than 4.5 MPa at 200–300 m along the strike. The stress on the top of the coal pillar decreases from the middle to both sides along the strike; at 100–200 m and 300–400 along the strike, the stress on the top of the coal pillar is less than that of the primary rock; At 100–150 m and 350–400 m along the strike of coal pillar, the *z*-direction stress direction changes (from z-down to z-up) in some areas, and the maximum value of the upward stress is approximately 0.5 MPa.

3.2 Z-displacement distribution coal pillars in different mining stages

Figure 8 the z-displacement distribution map of bottom surfaces of the coal pillar after the mining of working faces A, B, C and D. FLAC^{3D} specifies that the direction of the force is negative downward and positive upward along the *z*-direction.

3.2.1 Completion of stope A

The *z*-direction displacement of the bottom of the coal pillar increases from left to right, and the overall subsidence ranges between 0.01 and 0.15 m. The subsidence at the bottom of the coal pillar is less than that at the top, the whole coal pillar is in the compression state, and the compression at the left side of the coal pillar is the largest, with a compression of 0.1 m.

3.2.2 Completion of stope B

At this time, the *z*-direction displacement of the bottom of the coal pillar ranges between 0.17 and 0.34 m, which is slightly less than the *z*-direction displacement of the top of the coal pillar at this stage. The coal pillar is in the compression state, and the *z*-direction displacement of the bottom of the coal pillar is less than the middle on both sides (along the trend).

3.2.3 Completion of stope C

The *z*-direction displacement of the bottom surface of the coal pillar in the upper coal seam changes greatly due to the mining of working face C. 1) In the middle of the coal pillar, the entire coal pillar sinks approximately 3.6 m along the strike of 150–350 m, and the sinking area accounts for nearly 2/3 of the top slice of the whole coal pillar. 2) The *z*-direction displacement on the bottom of the coal pillar is basically symmetrical in the strike, and it decreases on both sides along the strike. At the

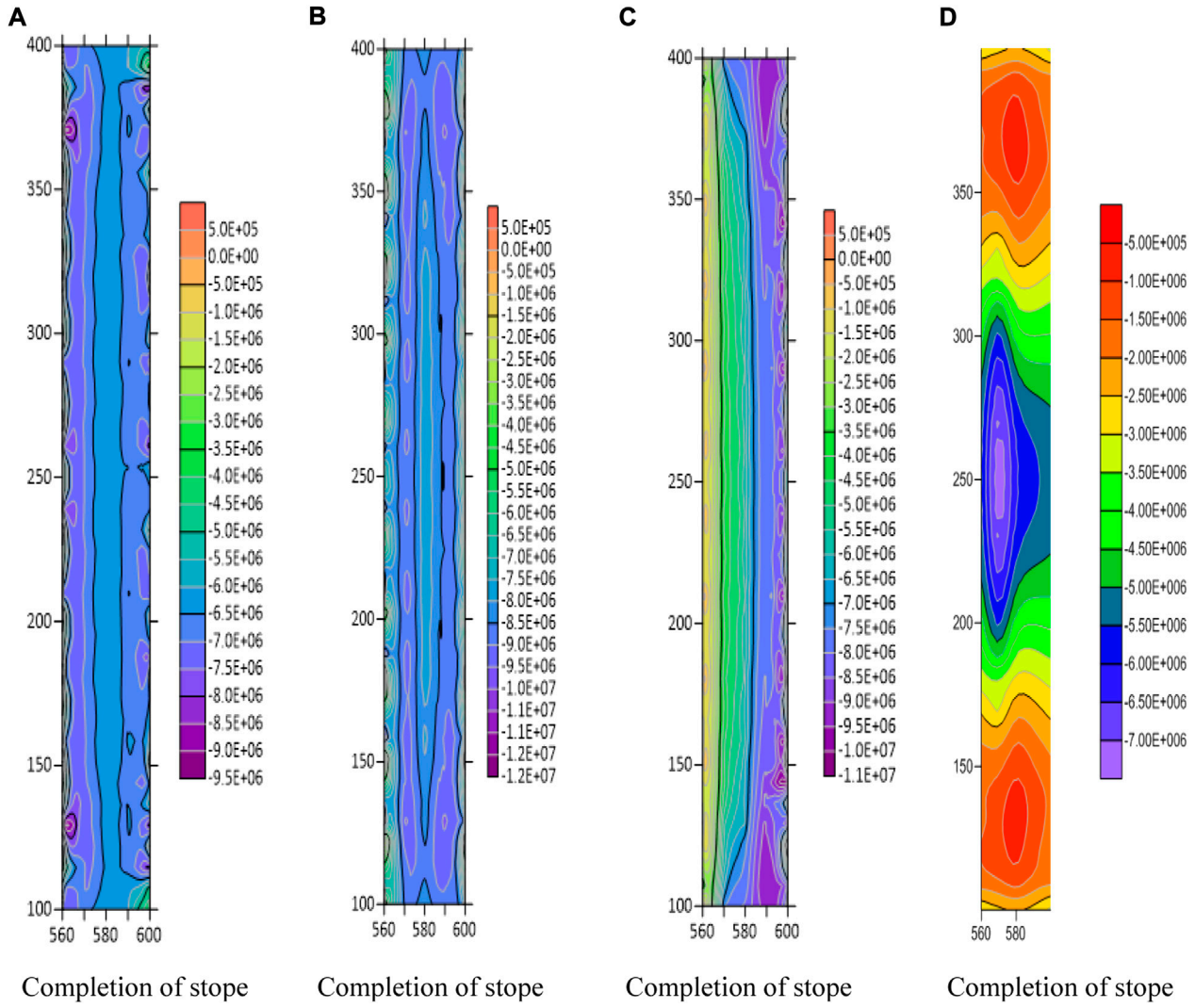

FIGURE 2
Z-Stress distribution of the top surface at different stages. Completion of stope **(A)**, **(B)**, **(C)** and **(D)** represent the mining of working face **(A)**, **(B)**, **(C)** and **(D)** respectively.

cutting hole, the minimum *z*-direction displacement on the bottom of the coal pillar is only approximately 0.4 m 3) The maximum relative z-displacement in the *Z* direction at the top of the coal pillar is 3.2 m. The recovery of face C is a process of pressure release for the coal pillar.

3.2.4 Completion of stope D

The *z*-direction displacement of the coal pillar bottom basically shows the same trend as the previous mining stage, with a large amount of decline in the middle and a small amount of decline on both sides along the strike. The mining of face D is a stress concentration process for the coal pillar, and the coal pillar is further compacted after the mining of face D is completed.

3.3 Stability analysis of the upper coal pillar

According to the calculation of A.H Wilson's empirical formula, it is considered that the coal pillar maintains good stability after the completion of mining faces A and B, the plastic failure area on the coal pillar is less than 20% of the whole coal pillar, and the coal pillar is in a stable state as a whole. Due to the particularity of repeated mining conditions of the close seam group, the A.H Wilson's empirical formula is not suitable for the stability judgement of the coal pillar after mining the adjacent layer below.

When the mining of face C is completed, the distribution diagram of the plastic area of the whole coal pillar is as follows in Figure 9:

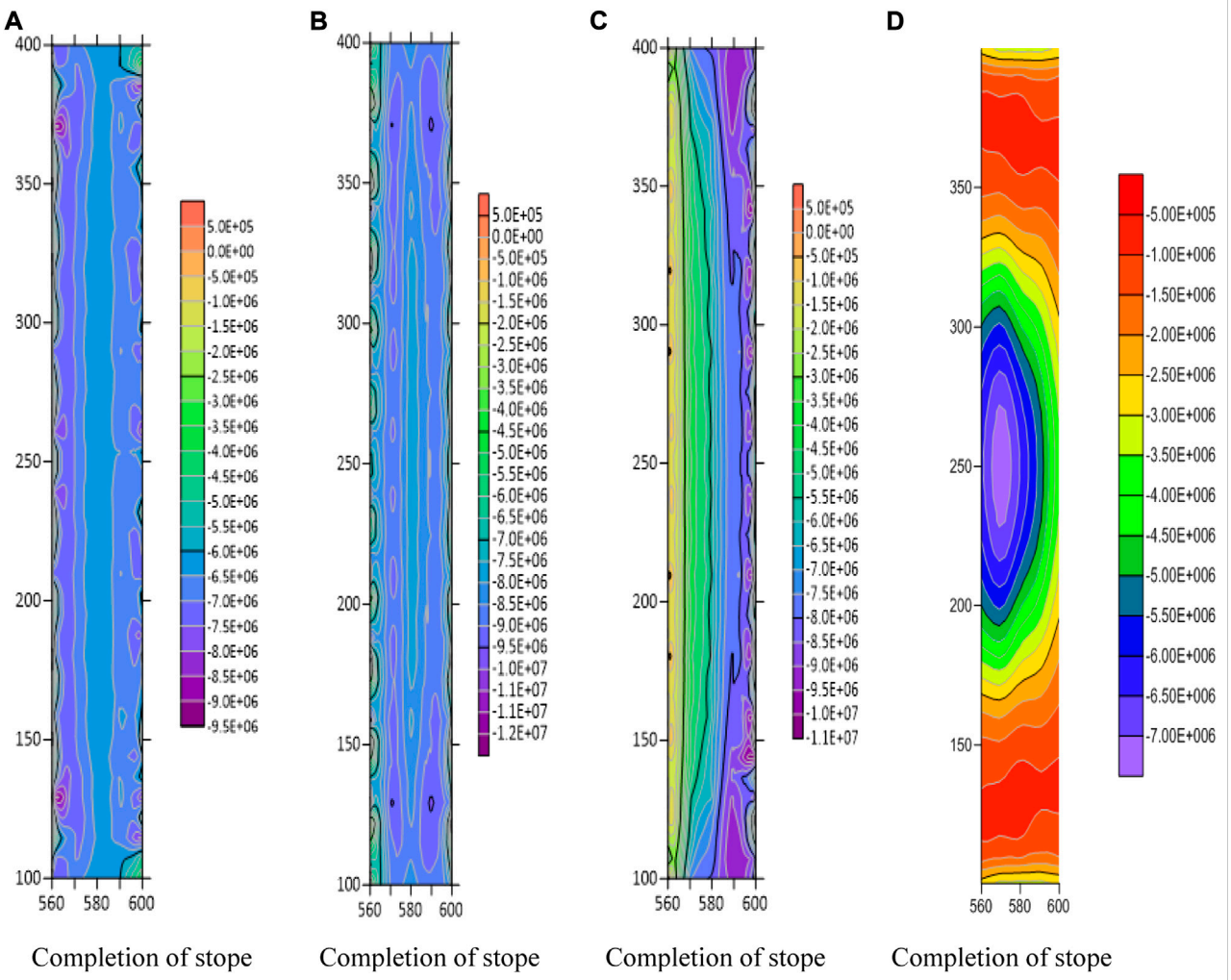

FIGURE 3
Stress distribution of the bottom surface in different mining stages. Completion of stope **(A)**, **(B)**, **(C)** and **(D)** represent the mining of working face **(A)**, **(B)**, **(C)** and **(D)** respectively.

In Figure 9, shear indicates shear failure, tension indicates tensile failure, - p indicates that the coal body in this area has experienced plastic failure in the past, and - n indicates that the coal body in this area is still in plastic failure state; as shown in the figure, when face C is fully recovered, the coal pillar is in a plastic state as a whole. The influence of the mining of the adjacent coal seam on its disturbance is not considered. It can be seen from the figure that the coal pillar has plastic damage due to the mining of coal face C. However, according to the analysis of the load strength of the coal pillar, the recovery of face C is a pressure relief process for the coal pillar (from the above analysis, it can be seen that the stress state of the whole coal pillar is greatly reduced after the completion of recovery of face C, but the coal pillar changes from the stable state at the end of recovery of face B to the unstable state after the completion of recovery of face C).

3.4 Breaking mechanism of coal pillar along strike

Therefore, in this paper, the author analyses the instability mechanism of coal pillar under the special conditions of repeated mining and staggered arrangement of coal pillars in shallow and short-distance coal seams in combination with the abovementioned changes of z-displacement and stress of coal pillars in different stages of mining.

It can be seen from Figures 10, 11 that with the continuous mining of face C, as the overburden rock continues to collapse towards the goaf of face C, when the hanging length of the coal pillar in upper coal seam exceeds a certain distance, the coal pillar will break along the strike, thus forming block articulated blocks G and H. At this time, it is not the excessive upper load that causes the collapse and instability of the coal pillar, but the

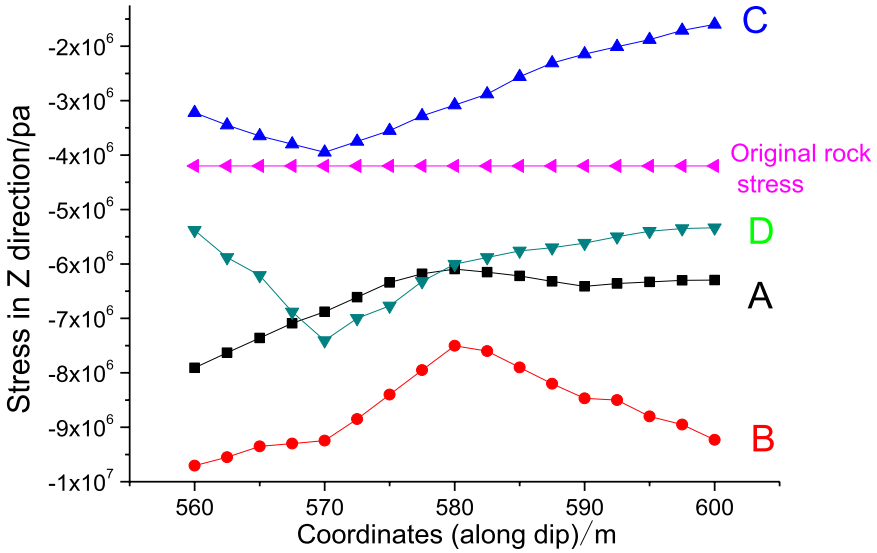

FIGURE 4
Stress variation at different mining stages (Y=250 m).

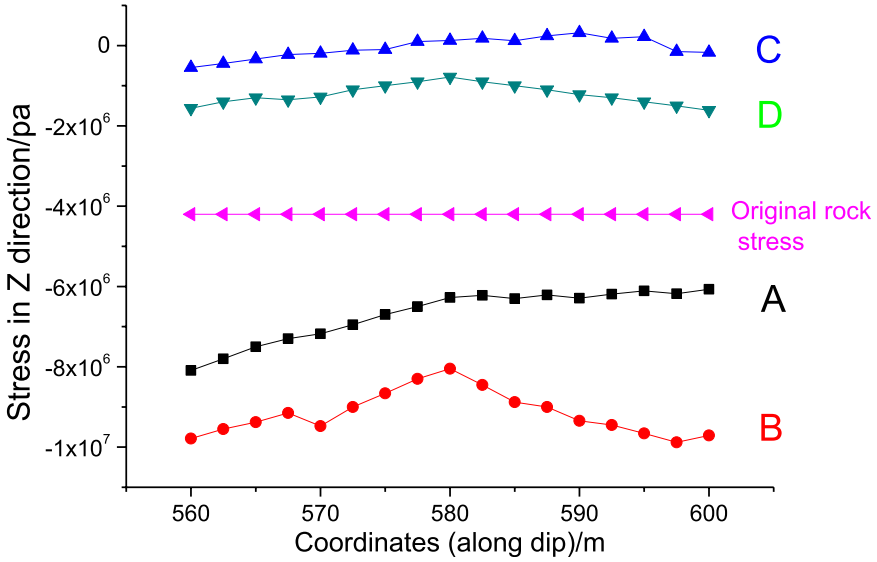

FIGURE 5
Stress variation at different mining stages (Y=140 m).

bedrock at the bottom of the coal pillar is affected by the mining of the lower coal seam, leading to the fracture and instability of the coal pillar along the strike. It can be seen from the above analysis that when the mining of face C is completed, there is a situation in which the stress direction on the coal pillar is along the *z*-axis. It is precisely because of the existence of this stress difference on the whole coal pillar that the coal pillar forms relative cutting along the strike, resulting in the fracture and instability of the coal pillar.

According to the above analysis, the "masonry beam" theory is used to analyse the coal pillar broken along the strike. At the moment when the coal pillar starts to break, the mechanical

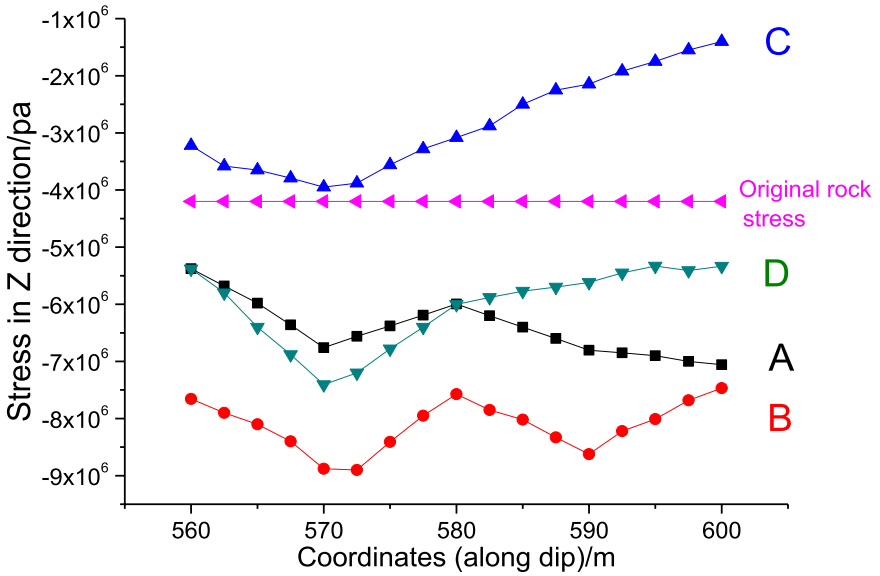

FIGURE 6
Bottom surface stress variation at different mining stages (Y=250 m).

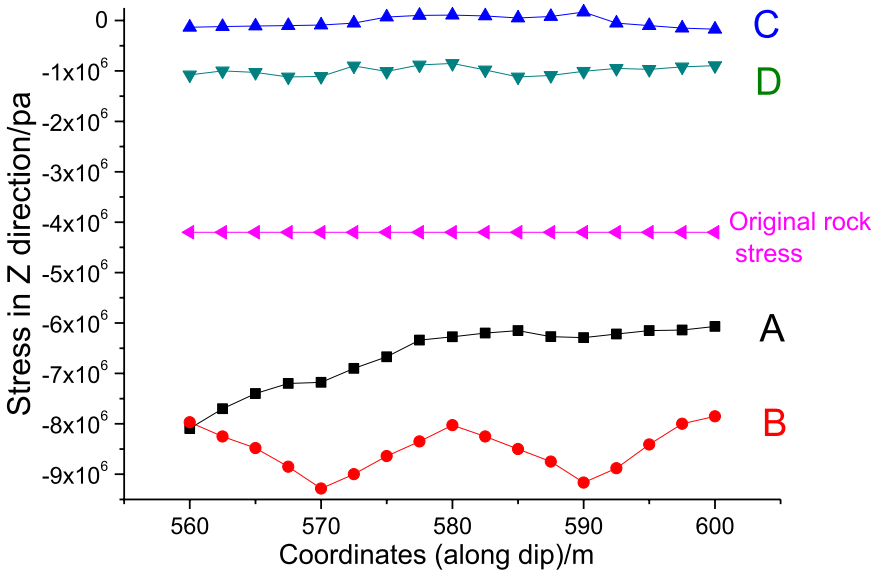

FIGURE 7
Bottom surface stress variation at different mining stages (Y=140 m).

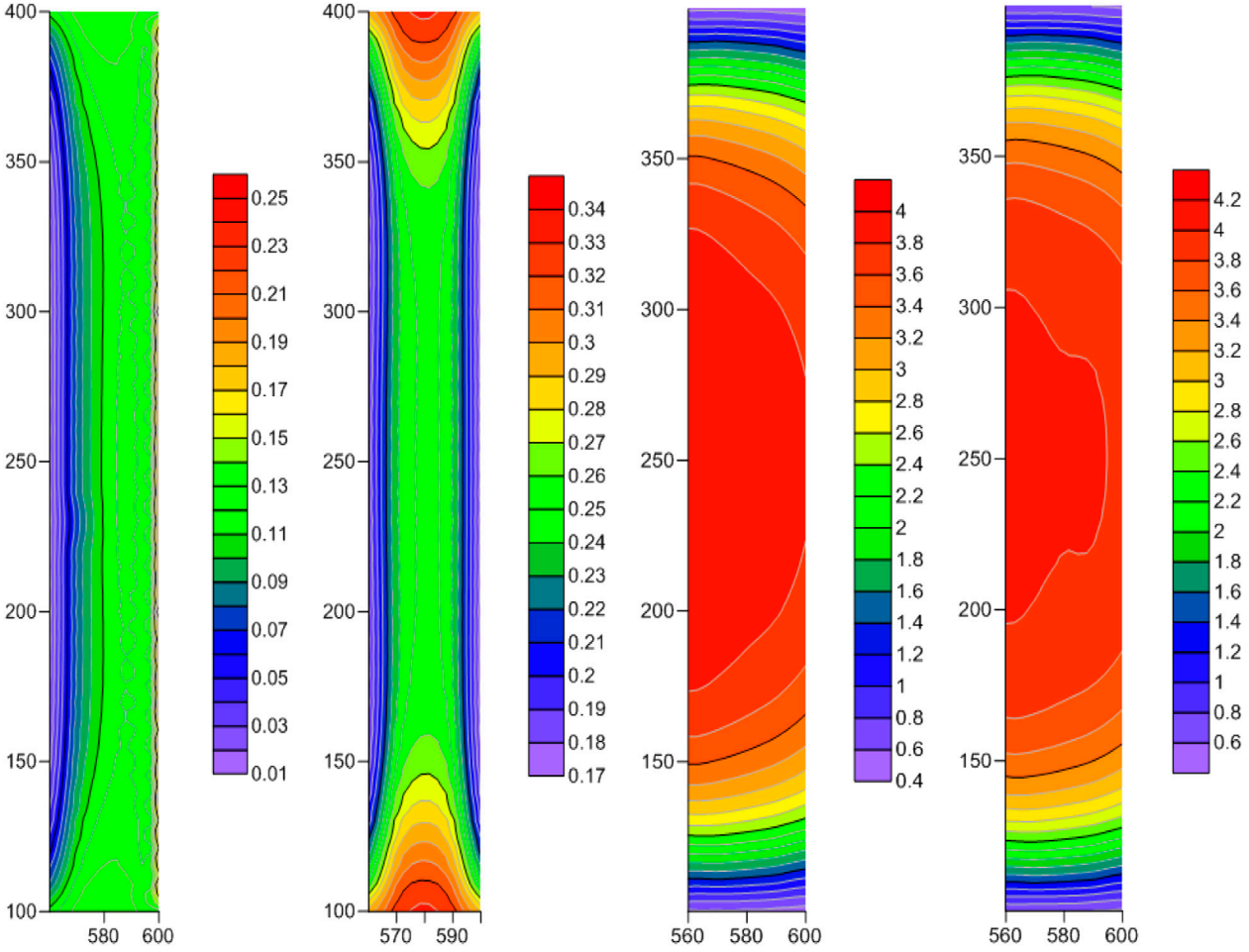

FIGURE 8
Z-displacement distribution at the bottom of the coal pillar in different mining stages.

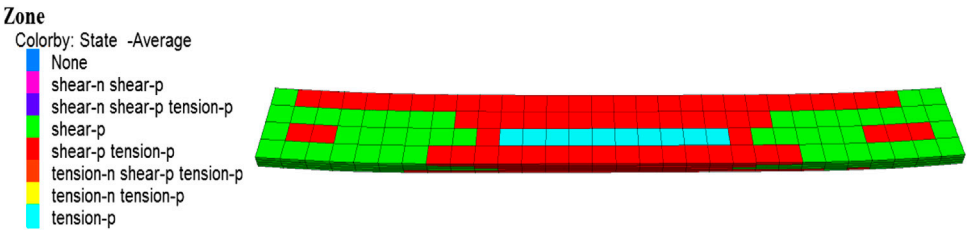

FIGURE 9
Plastic zone distribution of coal pillars after C recovery.

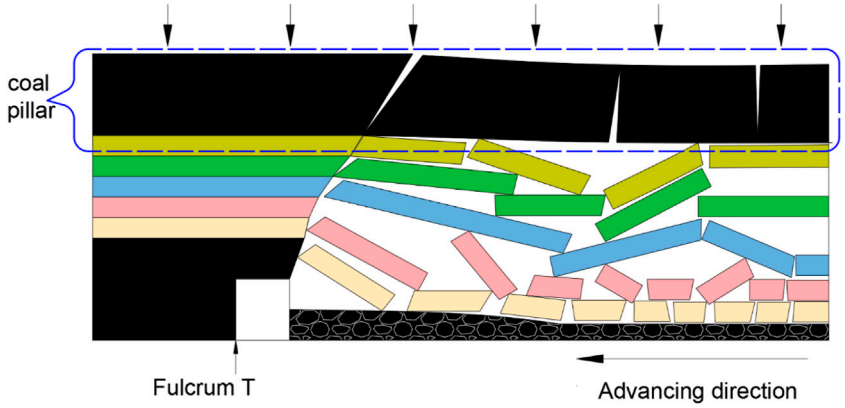

FIGURE 10
Section of the coal pillar along the trend at the stage of C recovery.

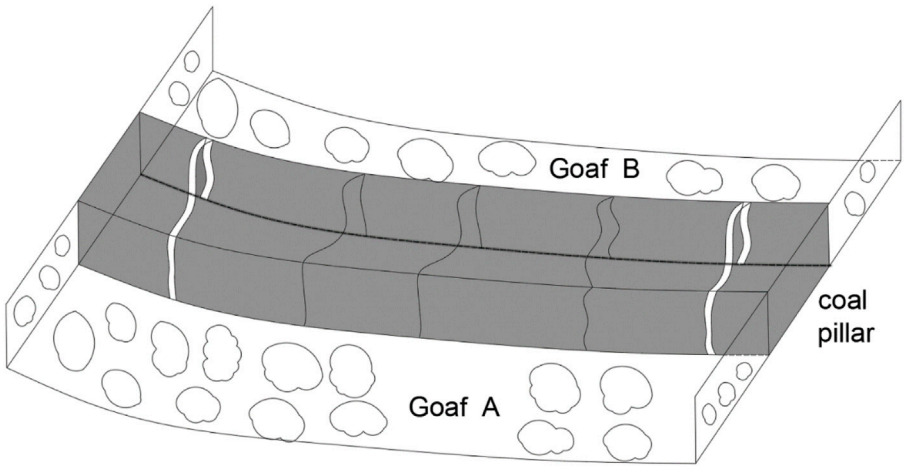

FIGURE 11
Fracture and instability diagram of coal pillar along strike.

model shown in Figure 12 is established for the key block G. Among them, F_B is the supporting force of coal pillar floor bedrock to coal pillar fracture block G. According to the moment balance relationship, it can be solved as follows:

$$F_B = \frac{1}{k_b}\left(R_H + \frac{1}{2}ql_g\right) \tag{1}$$

In the following formula: $\boldsymbol{l_g}$ is the length of the broken coal body $\boldsymbol{G}$; $\boldsymbol{R_H}$ is the shear stress of the hinge between the broken coal body $\boldsymbol{G}$ and $\boldsymbol{H}$; $\boldsymbol{q}$ is the load on the coal pillar; $\boldsymbol{k_b}$ is the coefficient, $\boldsymbol{k_b} = \boldsymbol{l_b}/\boldsymbol{l_g}$; and $\boldsymbol{l_b}$ is the strike distance of the supporting force $\boldsymbol{F_b}$ relative to the broken coal body boundary T.

In the above formula, $\boldsymbol{l_1}$ is the length of the broken coal pillar, $\boldsymbol{h_1}$ is the width of the broken coal pillar, and $\boldsymbol{\alpha}$ is the rotation angle of the broken coal rock mass H. Therefore, the above formula can be expressed as:

$$F_B = \frac{l_g}{l_b}\left[\frac{18 - 3l_1\sin\alpha}{18 - 2l_1\sin\alpha}ql_1 + \frac{1}{2}ql_g\right] \tag{2}$$

Then, the expression of L1 is obtained as follows:

$$l_1 = \frac{2k\sin\alpha + 18q + \sqrt{4k^2\sin^2\alpha + 342q^2 - 114k\sin\alpha}}{69\sin\alpha} \tag{3}$$

Combined with the z-direction displacement of coal pillars in different stages of mining, it can be well explained that the coal pillar in the upper coal seam will have stepped subsidence when the coal pillars are staggered outside. Combined with the z-direction displacement of coal pillars in different stages of

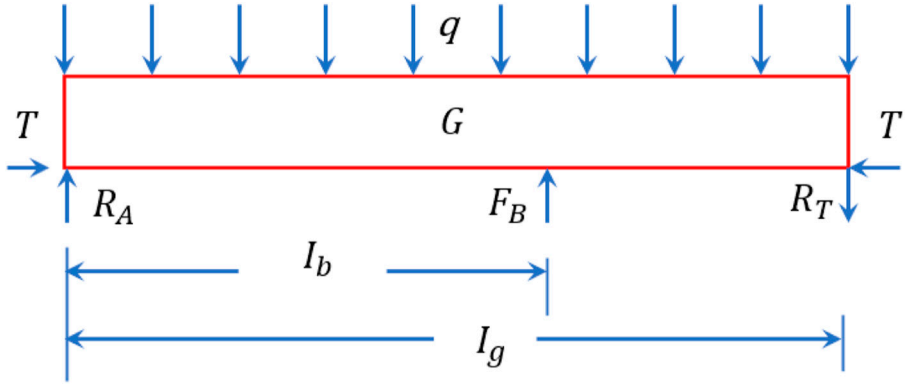

FIGURE 12
Mechanical model of broken coal G column.

TABLE 3 Coal pillar state at different stages.

Stage	Maximum z stress/MPa	Maximum Z displacement/m	Width of plastic zone/m	Pillar state
A	8.5	0.25	1.4	Stable
B	11.4	0.43	3.54	Stable
C	3.8	4	40	Breaking and stability
D	7	4.2	40	Compaction after breaking

mining, it can be well explained that when the coal pillars are staggered outside, mining below the adjacent coal seam will make the coal pillar of the upper coal seam sink step by step, which will lead to the relative cutting of coal pillars along the strike, which can also explain that at mining stage C, the load of the coal pillar is less than the original rock stress, but the coal pillar has a large area of plastic failure and instability. The status of coal pillars in different stages of mining is shown in Table 3 below:

3.5 Determination of hazardous area of coal pillar

According to the above analysis, different from the traditional coal pillar, which is broken and unstable because of the load exceeding the bearing limit, under the research conditions of this paper, the mining of the lower coal seam leads to the collapse of the bedrock under the coal pillar of the upper coal seam. After the completion of mining face C, the distribution diagram of displacement and stress on the top of the coal pillar is as follows:

According to the displacement, the coal pillar area is divided. Area A and C at both ends of the coal pillar along the strike are defined as the "step sinking area". The difference of the top surface is mainly concentrated in areas A and C. As shown in Figure 13 (1), due to the existence of a *z*-direction displacement difference, fractures along the dip are mostly developed in areas A and C, and the length of A and C is approximately 50 m, which is also consistent with the ultimate fracture length along the strike derived in this paper. B in the middle of the coal pillar is defined as "compaction after breaking". According to Figure 13 (1), the *z*-direction displacement difference of the coal pillar in this area can be ignored after compaction by overburdening. Area B is in the compaction state after breaking, and the fracture development degree and quantity in area B are far less than those in areas A and C. As shown in Figure 13 (2), area D is defined as the "reverse stress area". In area D, the stress on the top of the coal pillar appears to be vertical upward along the *z*-direction, which is opposite to the stress direction of other areas of the coal pillar, which is downward along the *z*-direction; the maximum *z*-direction stress difference between the coal body in area D and the middle of the coal pillar is 4 MPa, and the relative shear action of the coal pillar is obvious.

(Pan et al., 2017) conducted a temperature programmed test on unloading coal bodies with different initial stresses and concluded that unloading coal bodies are easier to oxidize than

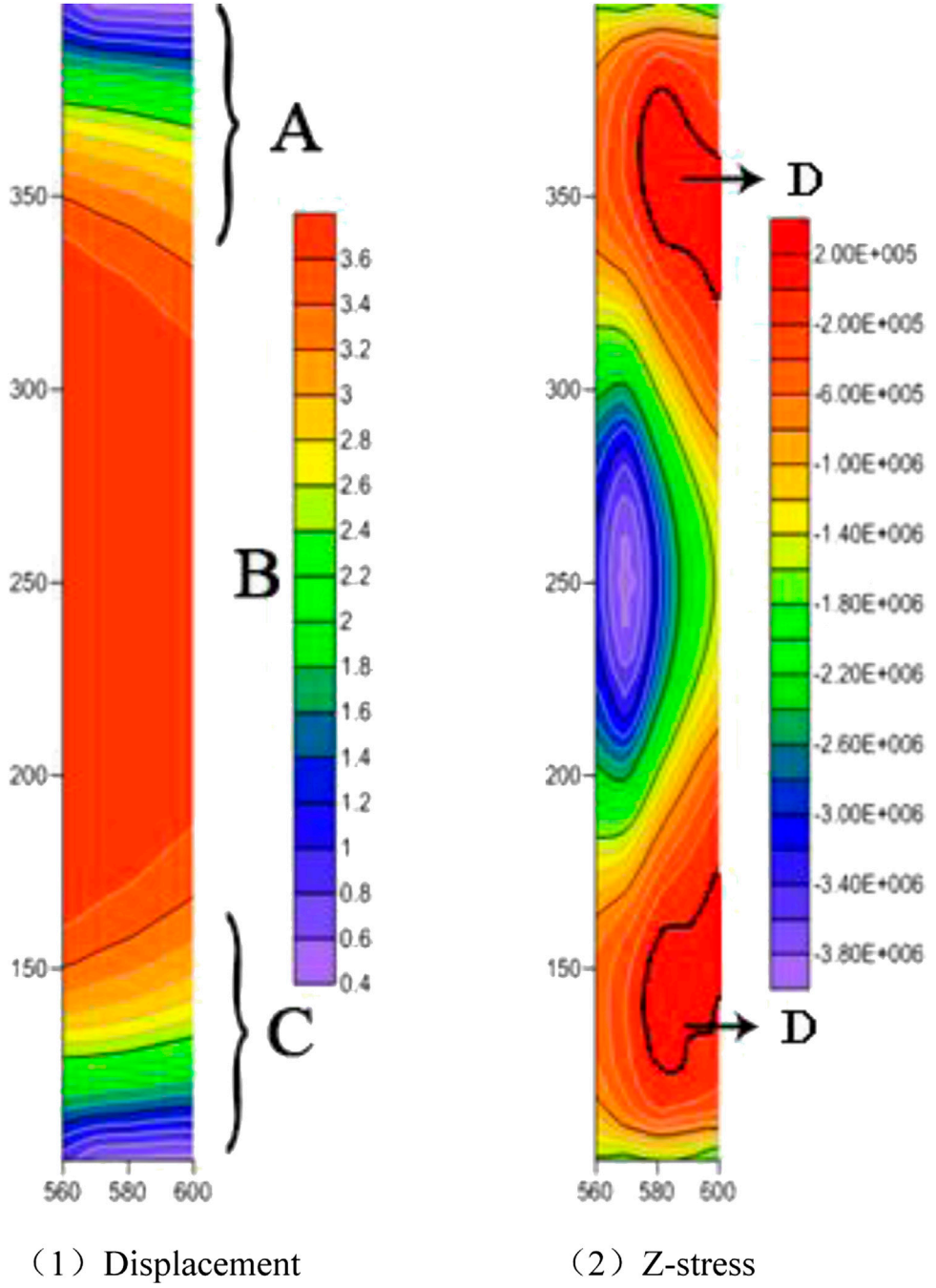

FIGURE 13
Distribution diagram of displacement and z-stress on top of coal pillar in old goaf after completion of stope D.

the original coal samples under different initial stresses. Under the research conditions in this paper, the stress on the coal pillar experienced three states: the original rock stress state, the stress concentration state and the stress release state. The load of the coal body in area D is only 0.05 times that of its original rock stress, which is approximately the state of complete unloading. In addition, most of area D coincides with area A with a fully developed fracture, so it can be determined that area D is a high-risk area for the spontaneous combustion of coal pillars in the upper coal seam under the condition of repeated mining of shallow buried coal seams.

4 Conclusion

In this paper, FLAC^{3D} numerical simulation software is used to simulate the repeated mining process of shallow buried and close-seam groups. Based on the analysis of the dynamic evolution process of the stress displacement of the upper coal pillar in different stages of mining, the mechanism of the instability and fracture of the upper coal pillar under the condition of the repeated mining of the shallow buried andxclose coal seam group is obtained. The conclusions are as follows:

1) In the process of repeated mining of a close coal seam group, the mining of the lower adjacent layer is a pressure relief process for the upper coal pillar. Compared with the traditional coal pillar, which is broken and unstable due to the load exceeding the ultimate strength, the main reason for the fracture and instability of the upper coal pillar is the difference distribution of the stress on the upper coal pillar caused by the mining of the lower coal seam.
2) The " block structure of voussoir beam " is used to calculate the ultimate fracture length of the coal pillar along the strike under this working condition, which is consistent with the numerical simulation.
3) According to the dynamic evolution characteristics of displacement stress on coal pillars, the coal pillar of the upper coal seam is divided into “step subsidence area”, “compaction after broken area” and “reverse stress area”, and the high spontaneous combustion risk area of coal pillars is determined and identified by combining with previous studies, which is of great practical significance for understanding the spontaneous combustion of coal pillars of upper coal seams under the condition of repeated mining.

Data availability statement

The original contributions presented in the study are included in the article/Supplementary Material, further inquiries can be directed to the corresponding author.

Author contributions

All authors listed have made a substantial, direct, and intellectual contribution to the work and approved it for publication.

Funding

This work was financially supported by the research fund provided by the National Key Research and Development Program of China (2018YFC0807900), the National Scientific Foundation of China (51574111, 52004084), the Henan Province Key R&D and Promotion Special (Technology Tackling Key) Project (222102320124, 22210232006, 212102310388, 22210232006), The Key scientific research projects plan of colleges and universities in Henan Province (22A440005).

Conflict of interest

The authors declare that the research was conducted in the absence of any commercial or financial relationships that could be construed as a potential conflict of interest.

Publisher’s note

All claims expressed in this article are solely those of the authors and do not necessarily represent those of their affiliated organizations, or those of the publisher, the editors and the reviewers. Any product that may be evaluated in this article, or claim that may be made by its manufacturer, is not guaranteed or endorsed by the publisher.

Supplementary material

The Supplementary Material for this article can be found online at: https://www.frontiersin.org/articles/10.3389/feart.2022.991304/full#supplementary-material

References

Asadi, A., Shahriar, K., and Goshtasbi, K. (2005). Development of a new mathematical model for prediction of surface subsidence due to inclined coal-seam mining[J]. *Journal- South Afr. Inst. Min. Metallurgy* 105 (1), 15–20.

Bi, Y., Xie, L., Wang, J., Zhang, Y., and Wang, K. (2019). Impact of host plants, slope position and subsidence on arbuscular mycorrhizal fungal communities in the coal mining area of north-central China. *J. Arid Environ.* 163, 68–76. doi:10.1016/j.jaridenv.2018.11.011

Changchun, H., and Jialin, X. (2018). Subsidence prediction of overburden strata and surface based on the Voussoir beam structure theory[J]. *Advances in Civil Engineering* 2018, 1–13. doi:10.1155/2018/2606108

Chen, C., Hu, Z., Wang, J., and Jia, J. (2019). Dynamic surface subsidence characteristics due to super-large working face in fragile-ecological mining areas: A case study in shendong coalfield, China. *Adv. Civ. Eng.* 2019, 1–16. doi:10.1155/2019/8658753

Cheng, W., Hu, X., Xie, J., and Zhao, Y. (2017). An intelligent gel designed to control the spontaneous combustion of coal: Fire prevention and extinguishing properties. *Fuel* 210, 826–835. doi:10.1016/j.fuel.2017.09.007

Genc, B., and Cook, A. (2015). Spontaneous combustion risk in South African coalfields. *J. South Afr. Inst. Min. Metallurgy* 115 (7), 563–568. doi:10.17159/2411-9717/2015/V115N7A1

Guo, H., Yuan, L., Shen, B., Qu, Q., and Xue, J. (2012). Mining-induced strata stress changes, fractures and gas flow dynamics in multi-seam longwall mining. *Int. J. Rock Mech. Min. Sci. (1997).* 54, 129–139. doi:10.1016/j.ijrmms.2012.05.023

Hao, M., Li, Y., Song, X., Kang, J., Su, H., and Zhou, F. (2019). Hazardous areas determination of coal spontaneous combustion in shallow-buried gobs of coal seam group: A physical simulation experimental study. *Environ. Earth Sci.* 78 (1), 39. doi:10.1007/s12665-018-8010-5

Huang, Q., and Cao, J. (2019). Research on threefield evolution and rational coal pillar staggered distancein shallow buried closely spaced multi-seam mining[J]. *J. China Coal* 44 (3), 681–689.

Huang, Q., and Du, J. (2018). Coupling control of pillar stress and surface cracks in shallow coal seam group mining[J]. *J. China Coal* 43 (3), 591–598.

Jaiswal, A., and Shrivastva, B. K. (2009). Numerical simulation of coal pillar strength. *Int. J. Rock Mech. Min. Sci.* 46 (4), 779–788. doi:10.1016/j.ijrmms.2008.11.003

Ju, J. F., and Xu, J. L. (2015). Surface stepped subsidence related to top-coal caving longwall mining of extremely thick coal seam under shallow cover. *Int. J. Rock Mech. Min. Sci. (1997).* 78, 27–35. doi:10.1016/j.ijrmms.2015.05.003

Kidybinski, A., and Babcock, C. O. (1973). Stress distribution and rock fracture zones in the roof of longwall face in a coal mine. *Rock Mech.* 5 (1), 1–19. doi:10.1007/BF01246754

Li, H., Li, H., and Song, G. (2016). Physical and mechanical properties of the coal-bearing strata rock in shendong coal field. *J. China Coal Soc.* 41 (11), 2661–2671.

Li, S., He, X., and Li, S. (2013). Experimental research on strata movement and fracture dynamic evolution of double pressure-relief mining in coal seams group[J]. *J. China Coal Soc.* 38 (127), 2146–2152.

Li, Y., Wang, J., Chen, Y., and Wang, Z. (2019). Overlying strata movement with ground penetrating radar detection in close-multiple coal seams mining. *Int. J. Distrib. Sens. Netw.* 15 (8), 155014771986985. doi:10.1177/1550147719869852

Liu, Y. (2019). Experimental analysis of coal permeability evolution under cyclic loading[J]. *J. China Coal* 44 (8), 2579–2588.

Liu, Y., Hou, J., and Zhang, L. (2016). Permeability experiments of pore structure in coal matrix[J]. *J. China Coal* 41 (2).

Lu, Y., and Qin, B. (2015). Identification and control of spontaneous combustion of coal pillars: A case study in the qianyingzi mine, China. *Nat. Hazards (Dordr).* 75 (3), 2683–2697. doi:10.1007/s11069-014-1455-2

Ma, L., Du, X., and Wang, F. (2013). Water-preserved mining technology for shallow buried coal seam in ecologically-vulnerable coal field: A case study in the shendong coal field of China [J]. *Disaster Adv.* 6, 268–278.

Majdi, A., Hassani, F. P., and Nasiri, M. Y. (2012). An estimation of the height of fracture zone in longwall coal mining[J]. *J. Am. Chem. Soc.* 107 (14), 4343–4345.

Pan, R., Chen, L., and Yu, M. (2017). Oxidation characteristics of unloaded coal under different initial stress[J]. *J. China Coal* 42 (9).

Prucz, J. C., and Fu, S. H. (1989). Prediction of dynamic fracture modes in coal mining. *Int. J. Rock Mech. Min. Sci. Geomechanics Abstr.* 26 (2), 161–167. doi:10.1016/0148-9062(89)90004-1

Przylucka, M., Graniczny, M., and Kowalski, Z. (2015). *Identification and changes of subsidence basins caused by coal mining activity in upper silesia using satellite interferometeric data[C]*, Fringe Workshop (University of the Witwatersrand).

Ramani, R. V. (1997). A numerical simulation of spontaneous combustion of coal in goaf[M]. *Int. Mine Vet.Congr.* 6, 313–316. doi:10.1016/S0140-6701(97)85372-6

Wactawik, J. (1998). A numerical simulation of spontaneous combustion of coal in goaf[J]. *Fuel Energy Abstr.* 39 (1), 15–19. doi:10.1016/S0140-6701(97)85372-6

Wang, H., Dlugogorski, B. Z., and Kennedy, E. M. (2003). Analysis of the mechanism of the low-temperature oxidation of coal. *Combust. Flame* 134 (1-2), 107–117. doi:10.1016/S0010-2180(03)00086-5

Wang, K., Tang, H., Wang, F., Miao, Y., and Liu, D. (2019). Research on complex air leakage method to prevent coal spontaneous combustion in longwall goaf. *PLoS ONE* 14 (3), e0213101. doi:10.1371/journal.pone.0213101

Wang, Z., Fu, X., * Hao, M., Li, G., Pan, J., Niu, Q., et al. (2021). Experimental insights into the adsorption-desorption of CH4/N2 and induced strain for medium-rank coals. *J. Petroleum Sci. Eng.* 204, 108705. doi:10.1016/j.petrol.2021.108705

Wang, Z., Pan, J., * Hou, Q., Niu, Q., Tian, J., Wang, H., et al. (2018a). Changes in the anisotropic permeability of low-rank coal under varying effective stress in Fukang mining area, China. *Fuel* 234, 1481–1497. doi:10.1016/j.fuel.2018.08.013

Wang, Z., Pan, J., * Hou, Q., Yu, B., Li, M., and Niu, Q. (2018b). Anisotropic characteristics of low-rank coal fractures in the Fukang mining area, China. *Fuel* 211, 182–193. doi:10.1016/j.fuel.2017.09.067

Wattimena, R. K., Kramadibrata, S., Sidi, I. D., and Azizi, M. (2013). Developing coal pillar stability chart using logistic regression. *Int. J. Rock Mech. Min. Sci.* 58, 55–60. doi:10.1016/j.ijrmms.2012.09.004

Xie, H., and Zhou, H. (1999). Application of FLAC to predict gound surface displacements due to coal extraction and its comparative analysis[J]. *Chin. J. Rock Mech. And Eng.* 5 (4), 29–33.

Zhu, L., Jialin, X., Jinfeng, J., Zhu, W., and Xu, J. (2018). The effects of the rotational speed of voussoir beam structures formed by key strata on the ground pressure of stopes. *Int. J. Rock Mech. Min. Sci.* 108, 67–79. doi:10.1016/j.ijrmms.2018.04.041

Zhuo, H., Qin, B., Qin, Q., and Su, Z. (2019). Modeling and simulation of coal spontaneous combustion in a gob of shallow buried coal seams. *Process Saf. And Environ. Prot.* 131, 246–254. doi:10.1016/j.psep.2019.09.011